Interaction of the Catch-Loop Tyrosine βY317 with the Metal at Catalytic Site 3 of *Chlamydomonas* Chloroplast F_1-ATPase†

Wei Chen and Wayne D. Frasch*

The Center for the Study of Early Events in Photosynthesis, Arizona State University, Tempe, Arizona 85287-1601

Received March 21, 2001

ABSTRACT: Site-directed mutants Y317C, Y317E, Y317F, Y317G, and Y317K were made to the catch-loop tyrosine on the β subunit of the chloroplast F_1-ATPase in *Chlamydomonas*. EPR spectra of VO^{2+}−ATP bound to site 3 of CF_1 from wild type and mutants were obtained. Every mutant changed the ^{51}V hyperfine parameters of the VO^{2+} bound at this site in the catalytically active conformation of the enzyme but had no effect on these parameters in the form that predominates when the enzyme activity is latent. These results indicate that this residue is a ligand to the metal of the Mg^{2+}−nucleotide complex that binds to the empty catalytic site. The mutations also decreased the k_{cat} of the ATPase activity to a much greater extent than k_{cat}/K_M. Thus, these mutations limit the rate of product (Mg^{2+}−ADP and phosphate) release in the ATPase direction or, conversely, the initial binding of substrates in the ATP synthesis direction. On the basis of these observations, coordination of βY317 by Mg^{2+}−ADP that binds to the empty catalytic site provides a means by which substrate binding could trigger γ subunit rotation and consequent conformation changes of β subunits during ATP synthesis.

Synthesis of ATP from ADP and phosphate takes place on the F_1[1] portion of the F_1F_o ATP synthase and is driven by F_o-mediated proton flux in response to a transmembrane proton gradient. A large part of the γ subunit of this enzyme exists as an α-helical coiled coil that extends the length of the core of F_1 formed by the surrounding three α and three β subunits (*1*−*3*). The γ subunit of purified F_1 rotates as a result of ATPase activity (*4*−*6*). Thus, during ATP synthesis, the F_o-mediated proton flux is believed to drive the rotation of the γ subunit to change the conformations of the three catalytic sites located primarily on the β subunits.

In the crystal structure of F_1 from bovine heart mitochondria (*1*) the three catalytic sites were in different conformations with one that contained Mg^{2+}−AMPPNP (β_{TP}), one that contained Mg^{2+}−ADP (β_{DP}), and one that was empty (β_E). During ATP synthesis, the binding of Mg^{2+}−ADP and phosphate to the empty catalytic site induces a conformational change so that the substrates become tightly bound (*7*). In this conformation, the equilibrium of bound substrates and products is close to unity. The two subsequent conformational changes of the catalytic site driven by the proton gradient decrease the affinity of the bound Mg^{2+}−ATP relative to that of Mg^{2+}−ADP. Consequently, the nonequilibrium proton gradient drives the formation of a nonequilibrium chemical gradient in which the cellular concentration ratio of ATP/ADP far exceeds that found at equilibrium. Because the conformations of the three catalytic sites are staggered, each of the conformations is present on the enzyme at any moment.

Nucleotides bind to the catalytic site as a complex with Mg^{2+} that serves as a cofactor for the reaction (*8*). The asymmetry of the catalytic sites necessary for the release of ATP against an unfavorable chemical gradient depends on Mg^{2+} as well as the γ subunit. In the absence of Mg^{2+} and the γ subunit, the crystal structure of the $\alpha_3\beta_3$ complex from the thermophilic *Bacillus* PS3 has 3-fold symmetry (*9*). In the rat liver mitochondrial F_1 structure which was crystallized in the absence of Mg^{2+}, the $\alpha_3\beta_3$ portion of the structure shows 3-fold symmetry despite the presence of the γ subunit (*2*). In the absence of Mg^{2+}, the three catalytic sites bind ATP with the same affinity (*10*). However, when ATP binds as a complex with Mg^{2+}, the affinity for nucleotides between the catalytic site conformations can differ by as much as 5 orders of magnitude. This suggests that the differences in affinity may in part result from changes in the metal ligands during the conformational changes at the catalytic sites.

Magnesium is difficult to study due to the lack of spectroscopic probes and is difficult to distinguish from water in a crystal structure. Vanadyl $(V^{IV}{=}O)^{2+}$ provides a direct probe of the types of groups that serve as ligands to the F_1 metal cofactor (*11*−*13*) because the *A* and *g* tensors derived from the EPR spectrum of the bound VO^{2+} are a direct measure of the nature of the equatorial metal ligands (*14*). The observation that site-directed mutations of a metal ligand change the ^{51}V hyperfine parameters of the EPR spectrum of F_1-bound VO^{2+} in a perceptible and predictable manner provided a means to identify specific residues as metal ligands (*15*).

† This work was supported by National Institutes of Health Grant GM50202.

* To whom correspondence should be addressed. E-mail: frasch@asu.edu. Tel: (480) 965-8663. Fax: (480) 965-6899.

[1] Abbreviations: AMPPNP, adenylyl imidodiphosphate; F_1, the extrinsic membrane portion of the F_1F_o ATP synthase; CF_1, chloroplast F_1; P-loop, phosphate-binding loop also known as the Walker homology A sequence; VO^{2+}, vanadyl; WHB, Walker homology B sequence; catch loop, MF_1 residues βY311−319.

10.1021/bi0105779 CCC: $20.00
Published on Web 06/01/2001

A variety of metals will function as cofactors for the F_1F_o ATP synthase (*16*). They are divided into either the Mg^{2+}-type or the Ca^{2+}-type group. In the presence of Mg^{2+}, F_1F_o can catalyze proton-gradient-driven ATP synthesis, and Mg^{2+}-dependent ATP hydrolysis pumps protons in the opposite direction. Concentrations of Mg^{2+} in excess of ATP inhibit activity. In the presence of Ca^{2+}, ATP synthase and ATPase-driven proton pumping do not occur. However, rates of ATPase activity of purified F_1 are higher with Ca^{2+} than with Mg^{2+}. Vanadyl falls in the Mg^{2+} group (*17*) along with Co^{2+}, Mn^{2+}, and Zn^{2+} (*16*).

Chloroplast F_1 retains nucleotides bound tightly at four sites upon purification (*18*). Each of these sites has unique characteristics that allow them to be depleted and filled with Mg^{2+}−nucleotide selectively (*19*). Nucleotide sites 1, 3, and 4 are catalytic while CF_1 site 2 is a noncatalytic site. The most extensive characterization of metal ligands using VO^{2+} EPR spectroscopy has been of CF_1 site 3 (*11*−*13*, *15*, *20*, *21*). This site has the lowest affinity for nucleotide and, thus, is likely to correspond to the empty catalytic site in the MF_1 crystal structure (*1*). As a result, little is known about this site from crystallographic methods.

The ATPase activity of CF_1 is latent upon purification from F_o and the thylakoid membranes but can be activated by reduction of a disulfide on the γ subunit. In the latent form, the predominant EPR species observed when VO^{2+}−ADP complex is tightly bound to site 3 is known as species B (*12*, *13*). Under these conditions, the Walker homology B-aspartate (βD262 in *Chlamydomonas* CF_1) was identified as a metal ligand at site 3 (*21*). The P-loop threonine (βT168 in *Chlamydomonas* CF_1) is not a metal ligand in site 3 of latent CF_1 but becomes a ligand in lieu of the Walker homology B-aspartate upon activation when the EPR signal intensity from species B is converted to species C (*15*).

We now report that mutations of the catch-loop tyrosine (βY317 in *Chlamydomonas* CF_1) change the ^{51}V hyperfine tensors of EPR species C, indicating that this residue is a metal ligand when VO^{2+}−nucleotide is bound to the activated form of site 3 (β_E). In the bovine MF_1 crystal structure, the β_E catch-loop residues $MF_1\beta$D316, $MF_1\beta$T318, and $MF_1\beta$D319 hydrogen bond to γ subunit residues $MF_1\gamma$R254 and $MF_1\gamma$Q255. Thus, these results show a direct link between the binding of Mg^{2+}−nucleotide to the empty catalytic site and the γ subunit. This link between the Mg^{2+} ligand and the γ subunit provides a possible escapement mechanism during ATP synthesis to ensure that expenditure of the protonmotive force to drive the rotation of the γ subunit only occurs when substrates bind to the empty catalytic site.

EXPERIMENTAL PROCEDURES

Construction of CF_1 Mutants in Chlamydomonas reinhardtii. The βTyr317 mutants were made as described by Chen et al. (*15*). The Chameleon mutagenesis kit (Stratagene) was employed to generate *atp*B mutations on pBam10.3-spec following the provided protocol using two primers.

The mutagenesis primers were βY317C, $_{5'}$CAGGCTGTATGTGTACCGGCAGATGACC$_{3'}$, βY317E, $_{5'}$CAGGCTGTAGAAGTACCGGCAGATGACC$_{3'}$, βY317F, $_{5'}$CAGGCTGTATTTGTACCGGCAGATGACC$_{3'}$, βY317G, $_{5'}$CAGGCTGTAGGTGTACCGGCAGATGACC$_{3'}$, and βY317K, $_{5'}$CAGGCTGTAAAAGTACCGGCAGATGACC$_{3'}$. The selection primer that changed the restriction site *Xmn*I to *Bam*HI was Ps, $_{5'}$CGCCCCGAAGAACGGATCCCAATGATGAGCAC$_{3'}$.

Sequences of DNA were obtained using ABI PRISM automatic sequencing to confirm the mutations in the plasmids. The sequencing primer was $_{5'}$CCGTACAGCTCCTGCTTTCG$_{3'}$. The mutated plasmids were purified by cesium chloride ultracentrifugation and diluted to 1 mg/mL prior to storage at −20 °C.

Transformation of the DNA plasmid containing mutated *atp*B genes into *C. reinhardtii* CC-373 cells employed biolistic methods using the PDS-1000 particle delivery system (Du Pont-New England Nuclear) (*20*). Southern blots as per Sambrook et al. (*22*) using ^{32}P-labeled pBam10-spec as the probe were used as an initial screen to identify homoplasmic mutants. This was then confirmed by double-stranded DNA sequencing.

Biochemical Characterization of C. reinhardtii Mutants. Cell cultures were maintained for each *C. reinhardtii* strain as per Hu et al. (*21*). The growth curves of the mutants were determined by the change in optical density (cell scattering) at 720 nm under photoautotrophic conditions as per Hu et al. (*21*).

To measure light-induced proton gradient formation, thylakoid membranes were suspended in 50 mM Tricine, pH 8.3, and 50 mM KCl, and then diluted to a final chlorophyll concentration of 5 mg of chlorophyll/mL in 2 mL of reaction mixture that contained 50 mM Tricine, pH 8.3, 50 mM KCl, 10 mM dithiothreitol, 0.5 μg/mL valinomycin, and 0.5 μM 9-aminoacridine. Fluorescence quenching was measured at room temperature using a Spex FluoroMax-DM3000 with excitation at 400 nm and emission at 450 nm.

For PMS-dependent photophosphorylation measurements, the thylakoid particles were prepared as per Hu et al. (*21*). Samples were assayed in 1 mL of reaction mixture that contained 10 μg of chlorophyll of dark-adapted thylakoid membranes, 50 mM Tricine−NaOH (pH 8.0), 10 mM NaCl, 0.3 mM $MgCl_2$, 2 mM NaH_2PO_4, 0.3 mM ADP, 2.0×10^5 cpm [α-^{32}P]ADP, 50 mM dithiothreitol, and 0.08 mM phenazine methyl sulfate. The reaction mixtures were illuminated with an Oriel-66181 lamp at 25 °C. The reactions were stopped by the addition of 4% trichloroacetic acid (TCA). The ADP and synthesized ATP were separated using silica thin-layer chromatography in a solvent of ammonium hydroxide−2-propanol−water at a ratio of 11:7:2 (v/v/v). The amount of synthesized [α-^{32}P]ATP was determined using a phosphor storage screen (Molecular Dynamics).

To measure ATPase activity, ammonium sulfate-precipitated CF_1 was desalted using a 1 mL centrifuge column of Sephadex G-50 in 100 mM Tricine (pH 8.0), and then stored in 20 mM Tricine (pH 8.0), 10 mM KCl, 1 mM EDTA, and 5 mM ATP. The reaction mixture contained 20 mM Tricine (pH 8.0), 1 mM EDTA, 50 mM dithiothreitol, 2×10^3 cpm [α-^{32}P]ATP, and $MgCl_2$ and ATP to obtain final concentrations of 0.05−12 mM Mg^{2+}−ATP. The reactions were initiated by addition of 10 μg of CF_1, followed by incubation at 37 °C for 4 min. Then 4% TCA was added to stop the reactions. The ADP generated by CF_1 hydrolysis was separated from ATP using silica thin-layer chromatography as described above. The amount of [α-^{32}P]ADP was deter-

mined using a phosphor storage screen (Molecular Dynamics).

EPR Analyses. Isolation of soluble CF_1-ATPase from wild-type and mutant *Chlamydomonas* and the selective filling of VO^{2+}−ATP into site 3 were carried out as per Chen et al. (*15*). A Bruker 580E spectrometer with a TE_{102} rectangular standard cavity and a liquid nitrogen flow cryostat operated at 125 K was used for EPR experiments at X-band (9 GHz). Of the eight transitions that result from that fraction of enzyme-bound VO^{2+} where the axis (defined by the oxo bond) is aligned parallel with the magnetic field, the $-7/2_{||}$, $-5/2_{||}$, $+3/2_{||}$, $+5/2_{||}$, and $+7/2_{||}$ transitions do not overlap with the perpendicular transitions. The measurable parallel transitions are distributed over a magnetic field range well in excess of 1000 G, and the high nuclear spin multiplicity of ^{51}V amplifies any discrepancy between simulated and observed field positions for these transitions. Therefore, a set of hypothetical $A_{||}$ and $g_{||}$ values, derived from a simulation that fits all five transitions well, can reasonably be expected to be both unique and quite accurate. Simulations of the EPR spectra employed the program QPOWA (*23*).

To estimate the types of groups that serve as equatorial ligands to VO^{2+} in each mutant, the observed values of $A_{||}$ derived from simulation of the EPR spectrum were compared with values of $A_{||}$ calculated from the coupling constants obtained from model studies (*14*, *24*) by

$$A_{||\mathrm{calc}} = \sum n_i A_{||i}/4 \qquad (1)$$

where i counts the different types of equatorial ligand donor groups, n_i ($n_i = 1-4$) is the number of ligands of type i, and $A_{||i}$ is the measured coupling constant for an equatorial ligand donor group of type i (*14*). Similar equations can be written for $g_{||}$.

RESULTS

Effects of the Mutations on Enzyme Assembly and ATP Synthesis. The yield of CF_1 purified from each *Chlamydomonas* βY317 mutant was approximately the same as that isolated from the wild type. Preparations of the enzyme from each mutant contained all five subunits in approximately the same abundance as those of the wild type as determined by SDS−polyacrylamide gel electrophoresis. These results suggest that the mutations do not affect the synthesis and assembly of the enzyme significantly when cultures were grown on acetate.

The relative abilities of the mutant and wild-type strains of *Chlamydomonas* to grow under photoautotrophic conditions are summarized in Table 1. The site-directed mutants of βY317E, βY317G, and βY317K were essentially incapable of photoautotrophic growth. The βY317C mutant grew at 13% of the wild-type rate, and the βY317F mutant grew at about the same rate as wild type in the logarithmic phase. The latter mutant was able to maintain this rate of growth longer than the wild type. The ability of thylakoids purified from *Chlamydomonas* to generate a proton gradient upon illumination was examined by measuring the fluorescence quenching of 9-aminoacridine (Table 1). No differences were observed between the wild type and mutants, which indicates that none of the thylakoids isolated from the mutants was uncoupled.

Table 1: Functional Comparison of Thylakoids from Wild Type and Mutants

strain	photoautotrophic growth rate[a] (%)	light-induced H^+-gradient formation[b] (%)	ATP synthase rate[c] (%)
wild type	100	100	100
Y317F	100	100	79
Y317C	13	100	6
Y317E	<1	100	3
Y317G	<1	100	1
Y317K	<1	100	2

[a] Cells were grown at 25 °C at a light intensity of 80 $\mu E \cdot M^{-2} \cdot s^{-1}$ and measured as optical density (cell scattering) of the liquid culture at 720 nm. [b] Light-driven proton gradient formation in thylakoids from *Chlamydomonas* measured by 9-aminoacridine fluorescence quenching. [c] Rates of PMS-dependent photophosphorylation in thylakoids from *Chlamydomonas*.

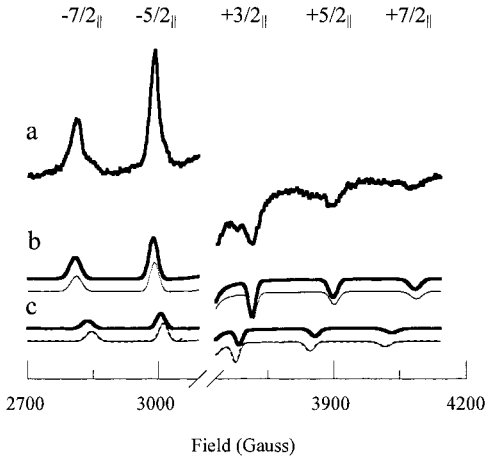

FIGURE 1: Parallel regions of VO^{2+} EPR spectra of the VO^{2+}−ATP complex bound to site 3 of CF_1βY317F (a). One mole equivalent of a 1:1 mole ratio of VO^{2+}−ATP was added to 70 mg of CF_1 that had been depleted of metal−nucleotide from site 3. EPR conditions were as follows: field modulation frequency, 100 kHz; modulation amplitude, 0.5 mT; sweep rate, 0.95 mT/s; time constant, 82 ms; microwave power, 2.0 mW; temperature, 125 K; microwave frequency, 9.40135 GHz; number of scans, 100. Simulated spectra of wild type (- - -) and mutant (—) for species B (b) and species C (c) were generated using the program QPOWA with the experimental conditions above and the ^{51}V hyperfine parameters from Table 2.

The rates of phenazine methyl sulfate-dependent photophosphorylation of thylakoids from the wild-type and mutant preparations are summarized in Table 1. The rates remained linear in all cases for up to 5 min. Even though the membranes were coupled to a similar extent as the thylakoids from the wild-type cells, the ATP synthase activities of βY317C, βY317E, βY317G, and βY317K were less than 10% of that of the wild type. The ATP synthase activity of βY317F was about 80% of the wild type. The results are consistent with the relative ability of each mutant to grow photoautotrophically.

Coordination of Metal at Site 3 in βY317 Mutants of CF_1. Catalytic site 3 of latent CF_1 was filled by the addition of 1 equiv of VO^{2+}−ATP in a 1:1 mole ratio. Figure 1a shows the parallel transitions that do not overlap with the perpendicular transitions in the EPR spectrum of VO^{2+} bound in this manner to the CF_1 from the βY317F mutant of *Chlamydomonas*. The types of groups coordinated at the equatorial positions of VO^{2+} strongly affect the magnitude

Table 2: VO^{2+} Coordination at Site 3 of CF_1 from Wild-Type and Mutant *Chlamydomonas*

strain	signal intensity ratio species C/B	experimental parameters[a]		calculated parameters[b]		most probable VO^{2+} equatorial ligands			
		$A_{\|\|}$ (MHz)	$g_{\|\|}$	$A_{\|\|}$ (MHz)	$g_{\|\|}$				
EPR species B									
WT		497.2	1.948	498.8	1.946	RCOO	P_i	H_2O	ROH
Y317F		497.2	1.948	498.8	1.946	RCOO	P_i	H_2O	ROH
Y317C		497.2	1.948	498.8	1.946	RCOO	P_i	H_2O	ROH
Y317E		497.2	1.948	498.8	1.946	RCOO	P_i	H_2O	ROH
Y317G		497.2	1.948	498.8	1.946	RCOO	P_i	H_2O	ROH
Y317K		496.2	1.949	498.8	1.946	RCOO	P_i	H_2O	ROH
EPR species C									
WT	0.87	456.5	1.958	456.3	1.958	ArOH	P_i	ROH	ROH
Y317F	0.21	467.0	1.955	467.8	1.954	RCOO	P_i	ROH	ROH
Y317C	0.43	452.4	1.960	449.7	1.962	RSH	P_i	ROH	RNH_2
Y317E	0.26	467.8	1.954	467.8	1.954	RCOO	P_i	ROH	ROH
Y317G	0.24	467.8	1.954	467.8	1.954	RCOO	P_i	ROH	ROH
Y317K	0.71	458.5	1.960	459.9	1.958	RNH_2	P_i	ROH	ROH

[a] Derived using QPOWA. [b] Calculated from eq 1.

of $g_{||}$ and $A_{||}$ that determine the position of the center of the parallel transitions and the spacing between them, respectively. Of these parameters, the coupling constant for the equatorial ligand donor group, $A_{||}$, shows the largest and most easily discerned changes as a function of the types of groups that serve as equatorial ligands.

Two sets of parallel transitions are observed from VO^{2+}−ATP bound to latent site 3 of βY317F−CF_1 (Figure 1a) that are similar to EPR species B and C reported previously for wild-type CF_1 (*12*, *13*). The simulated spectra for EPR species B and C from βY317F−CF_1 are shown as solid lines in spectra b and c of Figure 1, respectively. About 700 experimental data points were measured to define the region of the experimental spectrum shown where the parallel and perpendicular features do not overlap. Each data point in Figure 1a was signal-averaged 100 times (the result of 100 scans). Both the position and shape of the five independent spectral features in each EPR species in the experimental spectrum were fit by a single combination of $g_{||}$ and $A_{||}$ derived from the simulated spectrum, which are designated as experimental parameters in Table 2. The precision of the values of $A_{||}$ and $g_{||}$ depend on several factors including the sensitivity of the EPR cavity, the concentration of enzyme-bound VO^{2+}, and the number of scans that were signal-averaged. On the basis of 22 separate samples, the wild-type form of EPR species B was determined to have $A_{||} = 497.5 \pm 0.1$ MHz. The error inherent in the measurement of EPR species C was about the same.

Differences in the microwave frequency used to obtain a spectrum change the field positions at which the parallel transitions appear even though this does not affect the values of $g_{||}$ and $A_{||}$. The simulated spectra for EPR species B and C from wild-type CF_1 are shown as dashed lines in spectra b and c of Figure 1, respectively. The microwave frequency used in the experimental spectrum was used to generate both simulated spectra in order to provide a direct comparison of the changes in the EPR spectrum that result from the mutation. The parallel transitions of EPR species B from the mutant were the same as those of the wild type, indicating that the ^{51}V hyperfine components of species B remained unchanged. However, in species C, the parallel transitions of the mutant were clearly different from those of the wild type. The values of $A_{||}$ for EPR species C of the wild-type and βY317F enzymes differed by 10.5 MHz (Table 2).

The functional groups at the catalytic site that are available for metal ligation identified from the F_1 crystal structures (*1*, *2*) are all highly conserved in *Chlamydomonas* CF_1. Of these functional groups, four combinations that could serve as equatorial ligands in the Y317F mutant result in $A_{||}$ values of 459.89, 467.83, 468.06, and 476.60 MHz as calculated from eq 1. As shown in Table 2, the best fit of the experimental values of $g_{||}$ and $A_{||}$ for species C to those calculated by eq 1 was consistent with a group of ligands that differ from the wild type by single substitution of oxygen from either a carboxyl or phosphate group in lieu of the tyrosine hydroxyl group. The value of $A_{||}$ calculated from this ligand set differed from the experimental value by about 0.8 MHz.

The ratios of the amplitudes of the simulated spectra for EPR species B and C from each mutant that, when summed, reproduced the experimental spectrum are also shown in Table 2. These data provide the ratio of the amount of vanadyl bound in the form that gives rise to species B versus species C. The βY317F mutation decreased the signal intensity of species C relative to species B by about 4-fold.

From the data of Figure 2, the Y317C mutant decreased $A_{||}$ of species C by 4.1 MHz to a value of 452.4 MHz. A decrease in hyperfine coupling is anticipated from the incorporation of a sulfhydryl group as a ligand in exchange for an aromatic hydroxyl. However, a single substitution of this type is calculated from eq 1 to decrease $A_{||}$ by 21 MHz. The only set of equatorial ligands that satisfies the constraints of available ligands from the crystal structure and results in $g_{||}$ and $A_{||}$ values close to that observed for EPR species C from the Y317C mutant is shown in Table 2. This group of ligands includes coordination by a sulfhydryl and a second substitution where a lysine amino nitrogen becomes an equatorial ligand. Although the calculated value of $A_{||}$ for this ligand set from eq 1 deviates from the experimental value by 2.7 MHz, it is the only ligand set that fits with the ligands available in the catalytic site. It is noteworthy that when changes in the ^{51}V hyperfine tensors of VO^{2+} bound to catalytic site 3 were induced by site-directed mutations to βT168 and βD262, the cysteine mutation induced a second ligand substitution in addition to the coordination by the sulfhydryl (*15*, *21*).

The Y317C mutation also decreased the ratio of EPR species C/B by about 2-fold (Table 2). The change in the

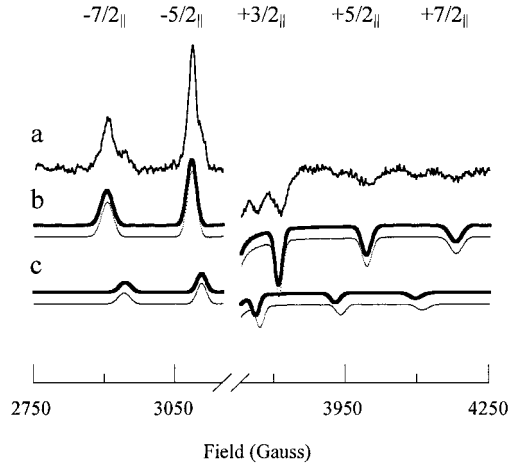

FIGURE 2: Parallel regions of VO^{2+} EPR spectra of the VO^{2+}−ATP complex bound to site 3 of $CF_1\beta$Y317C (a). One mole equivalent of a 1:1 mole ratio of VO^{2+}−ATP was added to 45 mg of CF_1 that had been depleted of metal−nucleotide from site 3. EPR conditions were as follows: field modulation frequency, 100 kHz; modulation amplitude, 0.5 mT; sweep rate, 0.95 mT/s; time constant, 82 ms; microwave power, 2.0 mW; temperature, 125 K; microwave frequency, 9.66183 GHz; number of scans, 200. Simulated spectra of wild type (- - -) and mutant (—) for species B (b) and species C (c) were generated as in Figure 1.

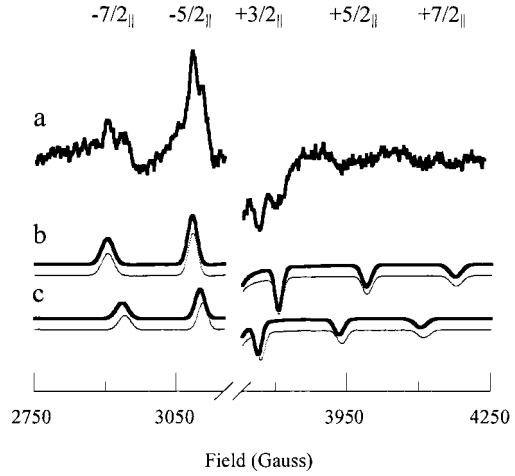

FIGURE 3: Parallel regions of VO^{2+} EPR spectra of the VO^{2+}−ATP complex bound to site 3 of $CF_1\beta$Y317K (a). One mole equivalent of a 1:1 mole ratio of VO^{2+}−ATP was added to 25 mg of CF_1 that had been depleted of metal−nucleotide from site 3. EPR conditions were as follows: field modulation frequency, 100 kHz; modulation amplitude, 0.5 mT; sweep rate, 0.95 mT/s; time constant, 82 ms; microwave power, 2.0 mW; temperature, 125 K; microwave frequency, 9.66025 GHz; number of scans, 300. Simulated spectra of wild type (- - -) and mutant (—) for species B (b) and species C (c) were generated as in Figure 1.

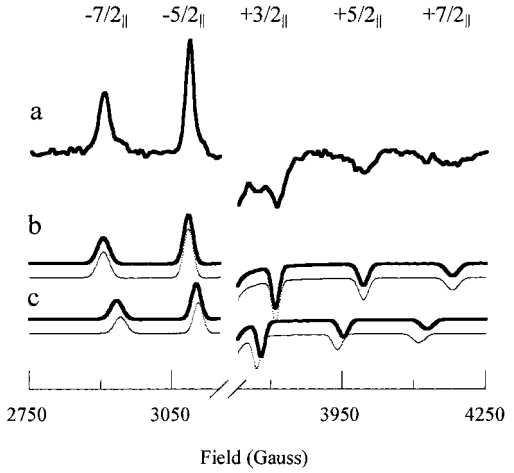

FIGURE 4: Parallel regions of VO^{2+} EPR spectra of the VO^{2+}−ATP complex bound to site 3 of $CF_1\beta$Y317G (a). One mole equivalent of a 1:1 mole ratio of VO^{2+}−ATP was added to 35 mg of CF_1 that had been depleted of metal−nucleotide from site 3. EPR conditions were as follows: field modulation frequency, 100 kHz; modulation amplitude, 0.5 mT; sweep rate, 0.95 mT/s; time constant, 82 ms; microwave power, 2.0 mW; temperature, 125 K; microwave frequency, 9.66393 GHz; number of scans, 280. Simulated spectra of wild type (- - -) and mutant (—) for species B (b) and species C (c) were generated as in Figure 1.

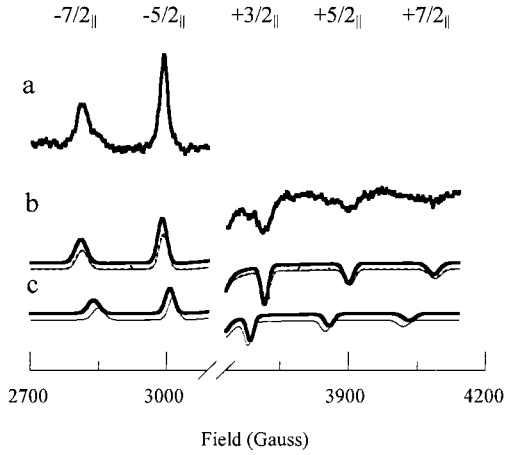

FIGURE 5: Parallel regions of VO^{2+} EPR spectra of the VO^{2+}−ATP complex bound to site 3 of $CF_1\beta$Y317E (a). One mole equivalent of a 1:1 mole ratio of VO^{2+}−ATP was added to 39 mg of CF_1 that had been depleted of metal−nucleotide from site 3. EPR conditions were as follows: field modulation frequency, 100 kHz; modulation amplitude, 0.5 mT; sweep rate, 0.95 mT/s; time constant, 82 ms; microwave power, 2.0 mW; temperature, 125 K; microwave frequency, 9.40536 GHz; number of scans, 200. Simulated spectra of wild type (- - -) and mutant (—) for species B (b) and species C (c) were generated as in Figure 1.

relative affinities for VO^{2+}−ATP bound in these two conformations is due solely to the changes in the ligands that give rise to EPR species C because this mutation did not affect the ^{51}V hyperfine parameters of EPR species B relative to wild type.

The EPR spectrum that resulted from VO^{2+}−ATP bound to site 3 of CF_1 with the Y317K mutation is shown in Figure 3. The ^{51}V hyperfine tensors of EPR species C increased as the result of the Y317K mutation while those of EPR species B remained unchanged. The value of $A_{\|}$ for a single ligand substitution of an amine for an aromatic hydroxyl calculated from eq 1 was about 1 MHz of the experimental value of species C in this mutant (Table 2). The second nearest ligand set allowable by the available groups in the crystal structure was calculated to have $A_{\|} = 467.83$ MHz. This mutation decreased the ratio of EPR species C/B by 0.16, which was the smallest change observed in any of the mutants.

Figures 4 and 5 show the effects of the Y317G and Y317E mutations, respectively, on the EPR spectra of VO^{2+}−ATP bound to site 3. These mutants effected the binding of VO^{2+}−ATP to site 3 in a closely similar manner. Neither mutant caused any changes in EPR species B. However, $A_{\|}$ of EPR species C decreased 11.3 MHz to a value of 467.8 MHz, consistent with a carboxyl or phosphate oxygen substituted for a tyrosine hydroxyl group as an equatorial

Table 3: Comparison of Kinetics Constants of Mg^{2+}−ATPase Activity of CF_1 from *Chlamydomonas* Wild Type and Mutants

strain	K_M[a]	V_{max}	k_{cat}	k_{cat}/K_M
WT	19.6	2.22	14.1	0.719
Y317F	12.8	0.71	4.5	0.352
Y317C	6.5	0.14	0.9	0.152
Y317E	5.9	0.16	1.0	0.169
Y317G	10.0	0.19	1.2	0.120
Y317K	23.8	0.19	1.2	0.050

[a] Units are as follows: K_M, mM; V_{max}, μmol of phosphate (mg of $CF_1)^{-1}$ min^{-1}; k_{cat}, s^{-1}; k_{cat}/K_M, s^{-1}·mM^{-1}.

metal ligand in like manner to the Y317F mutant. Both mutants also decreased the ratio of EPR species C/B by about 3.5-fold.

Effects of Mutations on ATPase-Related Function. The Mg^{2+}−ATPase activity of purified CF_1 from the wild-type and mutant strains of *Chlamydomonas* was determined as a function of substrate concentration. When plotted as a double reciprocal plot, the data from each mutant were linear. The kinetic constants of the ATPase activities are summarized in Table 3. In most cases, the mutations affected k_{cat} to a greater extent than k_{cat}/K_M. The k_{cat} and k_{cat}/K_M of βY317F decreased by 3- and 2-fold, respectively. The βY317C, βY317E, and βY317G mutants had k_{cat} and k_{cat}/K_M values that were 12−14-fold less and 4−6-fold less, respectively, than those of wild type. Only the βY317K mutant showed decreases in k_{cat} and k_{cat}/K_M that were about the same magnitude (14-fold).

DISCUSSION

The data presented here suggest that βY317 provides a direct link between initial substrate binding and the energy-driven conformational changes for three reasons. First, the βY317 mutations are rate limiting to the step of substrate binding to the empty site and its conversion to the tight site during ATP synthesis. In most every case, mutations at this residue decreased the k_{cat} of Mg^{2+}−ATPase activity to a much greater extent than k_{cat}/K_M. These data indicate that these mutants significantly limit the rate of product (Mg^{2+}−ADP and phosphate) release but have less effect on catalysis or substrate (Mg^{2+}−ATP) binding. Thus, in the ATP synthesis direction, this tyrosine is important for the intial binding of Mg^{2+}−ADP and phosphate and the first conformational change that results in tightly bound substrates. The binding of substrates to the empty catalytic site triggers the rotation of the γ subunit in response to the proton gradient (*7*) in an as yet undetermined way. This rotation in turn changes the conformation of each catalytic site.

Second, the results presented here show that βY317 is a metal ligand when Mg^{2+}−ATP binds to the activated form of site 3 of *Chlamydomonas* CF_1. All of the mutants examined here changed the ^{51}V hyperfine parameters of species C, the EPR species that arises from VO^{2+}−nucleotide bound to the activated and catalytically competent form, but had no effect on species B, the form that predominates in the latent, nonfunctional state. The decreases in the ratio of EPR species C/B observed for all mutants indicate that the binding of VO^{2+}−nucleotide to the functional species C form is less favorable in the mutants than in wild-type CF_1. It is noteworthy that the mutations caused similar changes in the ratio of species C/B as to the differences between k_{cat} and k_{cat}/K_M of the Mg^{2+}−ATPase activity. Site 3 of chloroplast F_1 is the catalytic site with lowest affinity for the metal−nucleotide complex, thereby making it equivalent to the empty (β_E) catalytic site of mitochondrial F_1. Thus, the effects of the mutations on ATPase kinetics and the EPR spectra of VO^{2+}−nucleotide binding to site 3 concur that this tyrosine is important for the initial binding of the metal−nucleotide complex to the empty catalytic site.

Third, βY317 provides a direct link between initial substrate binding and the energy-driven conformational changes due to its location. This tyrosine is the first residue of the catch loop that makes one of the three major contact points between the β and γ subunits. Hydrogen bonds between γ subunit residues $MF_1\gamma$R254 and $MF_1\gamma$Q255 and loop residues on β_E ($MF_1\beta$D316, $MF_1\beta$T318, and $MF_1\beta$D319) form a "catch" (*1*). This catch may prevent rotation of the γ subunit until the empty site fills with substrates, despite the exertion of constant torque by the proton gradient. In so doing, the dissipation of energy from the proton gradient would only be able to occur when the catalytic sites are filled, such that tight coupling between the gradient and ATP synthesis is maintained.

When the β_E site binds substrate as a complex with Mg^{2+}, ligation of the tyrosine by the metal may be sufficient to break the hydrogen bonds by deforming the loop, thereby triggering γ subunit rotation and conformational changes of all three catalytic sites. Because all three catalytic sites change conformation in response to the rotation of the γ subunit, rotation will necessarily induce one site to form the conformation that leads to product dissociation. Hydrogen bonds between the γ subunit and the catch loop of this newly formed β_E site would limit the γ subunit rotation to 120° per catalytic event. The evidence presented here is consistent with the participation of the catch-loop tyrosine (βY317) in an escapement mechanism commonly used in clocks to limit the expenditure of a constant applied force to the incremental movement of the hands. It is noteworthy that mutations to the equivalent of $MF_1\gamma$N256 or to DDLTD ($MF_1\beta$315−319) in the catch loop lowered the cooperativity of EF_1 catalysis and energy coupling (*25*).

While the data presented here clearly show that βY317 is a metal ligand at site 3, the retention of significant catalytic activity in the Y317F mutant also shows that metal ligation in itself is not a critical factor in the contribution of this residue to enzymatic activity. Although Y317F and Y317G are both incapable of providing a ligand to the metal and both have apparently formed the same equatorial ligands to the VO^{2+}−nucleotide, only Y317F has substantial catalytic function. The obvious difference between these residues is that phenylalanine has a large, hydrophobic side chain with substantial rigidity, while glycine essentially lacks a side chain and increases flexibility of the catch loop. The lack of catalytic function in the other mutants examined may also be explained by the absence of a large, rigid group at this position. Displacement of a bulky side chain by the metal−nucleotide may be sufficient to deform the catch loop enough to break the hydrogen bonds and allow the rotation of the γ subunit. It is very likely that this is one of a few groups on the enzyme involved with the coupling of substrate binding and γ subunit rotation-induced conformational changes.

It is noteworthy that His465 of the helicase domain from the helicase−primase of bacteriophage T7, which shares the

same structural core with the F_1 ATPase, occupies a position closely similar to the F_1 catch-loop tyrosine (*26*). The T7 helicase forms a hexameric ring of subunits around one strand of duplex DNA much like $F_1\alpha_3\beta_3$ surrounds the γ subunit (*27*, *28*). The unwinding of DNA by the T7 helicase results from dTTPase-driven rotation of this strand of DNA via a binding-change type mechanism in a manner similar to the ATPase-driven rotation of the γ subunit (*29*). On the basis of the position of T7 helicase−His465 in the loop that connects the metal−nucleotide binding site to the site of contact with the rotating DNA strand, this residue has been postulated to act as a conformational switch in rotation (*26*). Little is known about the binding site for the divalent metal that is a required cofactor for nucleotide hydrolysis in T7 helicase (*26*). Consequently, more work is required to determine if T7−His465 and $CF_1\beta$Y317 serve a similar function.

REFERENCES

1. Abrahams, J. P., Leslie, G. W., Lutter, R., and Walker, J. E. (1994) *Nature 370*, 621−628.
2. Bianchet, M. A., Hullihen, J., Pedersen, P. L., and Amzel, L. M. (1998) *Proc. Natl. Acad. Sci. U.S.A. 95*, 11065−11070.
3. Stock, D., Leslie, A. G. W., and Walker, J. E. (1999) *Science 286*, 1700−1705.
4. Duncan, T. M., Bulygin, V. V., Zhou, Y., Hutcheon, M. L., and Cross, R. L. (1995) *Proc. Natl. Acad. Sci. U.S.A. 92*, 10964−10968.
5. Sabbert, D., Engelbrecht, S., and Junge, W. (1996) *Nature 381*, 623−626.
6. Noji, H., Yasuda, R., Yoshida, M., and Kinosita, K., Jr. (1997) *Nature 386*, 299−302.
7. O'Neal, C. C., and Boyer, P. D. (1984) *J. Biol. Chem. 259*, 5761−5767.
8. Frasch, W. D., and Selman, B. R. (1982) *Biochemistry 21*, 3636−3643.
9. Shirakihara, Y., Leslie, A. G. W., Abrahams, J. P., Walker, J. E., Ueda, T., Sekimoto, Y., Kambara, M., Saika, K., Kagawa, Y., and Yoshida, M. (1997) *Structure 5*, 825−836.
10. Weber, J., Bowman, C., and Senior, A. E. (1996) *J. Biol. Chem. 271*, 18711−18718.
11. Houseman, A. L. P., LoBrutto, R., and Frasch, W. D. (1994) *Biochemistry 33*, 4910−4917.
12. Houseman, A. L., LoBrutto, R., and Frasch, W. D. (1994) *Biochemistry 33*, 10000−10006.
13. Houseman, A. L., LoBrutto, R., and Frasch, W. D. (1995) *Biochemistry 34*, 3277−3285.
14. Chasteen, N. D. (1981) in *Biological Magnetic Resonance* (Berliner, L., and Reuben, J., Eds.) pp 53−119, Plenum Press, New York.
15. Chen, W., LoBrutto, R., and Frasch, W. D. (1999) *J. Biol. Chem. 274*, 7089−7094.
16. Strid, Å., and Nyrén, P. (1989) *Biochemistry 28*, 9718−9724.
17. Frasch, W. D. (2000) *Biochim. Biophys. Acta 1458*, 310−325.
18. Shapiro, A. B, Huber, A. H., and McCarty, R. E. (1991) *J. Biol. Chem. 266*, 4194−4200.
19. Bruist, M. F., and Hammes, G. G. (1981) *Biochemistry 20*, 6298−9305.
20. Hu, C.-Y., Houseman, A. L. P., Morgan, L., Webber, A. N., and Frasch, W. D. (1996) *Biochemistry 35*, 12201−12211.
21. Hu, C.-W., Chen, W., and Frasch, W. D. (1999) *J. Biol. Chem. 274*, 30481−30486.
22. Sambrook, J., Fritsch, E. F., and Maniatis, T. (1989) in *Molecular Cloning, A Laboratory Manual*, p 9.31−9.55, Cold Spring Harbor Laboratory Press, Cold Spring Harbor, NY.
23. Mustafi, D., Telser, J., and Makinen, M. W. (1992) *J. Am. Chem. Soc. 114*, 6219−6226.
24. Hamstra, B. J., Houseman, A. L., Colpas, G. J., Kampf, J. W., LoBrutto, R., Frasch, W. D., and Pecoraro, V. L. (1997) *Inorg. Chem. 36*, 4866−4874.
25. Futai, M., and Omota, H. (1996) *J. Bioenerg. Biomembr. 28*, 409−414.
26. Sawaya, M., Guo, S., Tabor, S., Richardson, C. C., and Ellenberger, T. (1999) *Cell 99*, 167−177.
27. Patel, S. S., and Hingorani, M M (1993) *J. Biol. Chem. 268*, 10668−10675.
28. Yu, X., Hingoani, M M., Patel, S. S., and Engelman, E. H. (1996) *Nat. Struct. Biol. 3*, 740−743.
29. Manju, M., Hingorani, M. M., Washington, M. T., Moore, K. C., and Patel, S. S. (1997) *Proc. Natl. Acad. Sci. U.S.A. 94*, 5012−5017.

BI0105779